Broadband Metasurfaces with Simultaneous Control of Phase and Amplitude

Lixiang Liu, Xueqian Zhang, Mitchell Kenney, Xiaoqiang Su, Ningning Xu, Chunmei Ouyang, Yunlong Shi, Jiaguang Han,* Weili Zhang,* and Shuang Zhang*

Metamaterials have continuously attracted enormous interest due to their unusual electromagnetic properties, which can be utilized for engineering the electromagnetic space and controlling light propagation, with prominent examples including negative and zero refraction,[1–7] sub-diffraction imaging,[8–10] and invisibility cloaking.[11–13] Despite the success of metamaterials in ushering an array of new fundamental physics and potential applications, devising metamaterials for practical applications, however, still remains a big challenge. In particular, the material loss and fabrication challenges have roadblocked their transition to real world applications. For bulk metamaterials, this usually cannot be avoided due to the fact that metals are the primary constituent materials, whereby the ohmic loss of metals at optical frequencies is quite significant. Moreover, volumetric metamaterials very often require precise alignment between different layers, which poses a great challenge even with the most state-of-the-art nanofabrication tools. Recently, metasurfaces consisting of a monolayer of plasmonic structures, capable of controlling the wavefront of light, serve as an alternative approach to bypass the loss and fabrication issues, and open doors for bridging the gap between the fundamental research of the artificial structures and their device applications.[14–41] Being as thin as only a fraction of the wavelength, the optical loss is not a major concern. In addition, the complex and time-consuming alignment process necessary for fabrication of bulk metamaterials is not required. Despite being at its infancy, metasurfaces have shown great promise for novel device applications, as evidenced by the demonstration of a number of interesting devices, such as ultrathin metasurface flat lens,[20–22] high efficiency[23–25] and switchable surface plasmon couplers,[26,27] high resolution three-dimensional (3D) metasurface holograms,[28–32] and some other functional interfaces.[33–41]

Most of the metasurfaces demonstrated so far, however, are designed to manipulate only the phase profile of the output electromagnetic waves. Completely manipulating the propagation of light, on the other hand, requires simultaneous amplitude and phase control. In certain important applications, such as holography, laser beam shaping, and synthesis of complex wave fields, manipulation of both of these degrees of freedom is required to generate high quality holographic images. Attempts have been made to simultaneously engineer the phase and amplitude profiles of a metasurface through designing the geometry of antennas.[31–33] In Ref. [33], the complete control over phase and amplitude is realized in a detour phase scheme, where the pixel size of the diffractive surface is significantly greater than the wavelength of the light. Multilayer metasurfaces for such purpose was proposed in Ref. [32]; however, the alignment involved in such multilayer design would make its fabrication process highly complicated and challenging. A single layer metasurface with subwavelength pixel size was realized for engineering both phase and amplitude,[31] but it was limited to only a few discrete levels for both parameters, due to the complexity required in matching the antenna geometry to the desired values of phase and amplitude. The design is complicated by the fact that each combination of amplitude and phase corresponds to a different geometrical design of the antenna, which would unavoidably introduce less fabrication tolerances. Moreover, it is very difficult to achieve broadband operation with such a complicated design scheme. Here, a robust and facile approach is employed for achieving simultaneous phase and amplitude manipulation in a single layer metasurface over a broadband frequency range in the terahertz regime. In comparison to previous approaches, our metasurface design uniquely combines a number of important merits – subwavelength pixel size for continuous wavefront manipulation, easy fabrication, robust and broadband control of both the phase and amplitude, and in particular, the amplitude can be engineered precisely and continuously.

Our design combines the functionalities of two types of metasurfaces – a metasurface for phase control determined

L. Liu,[+] X. Zhang,[+] M. Kenney,[+] Prof. S. Zhang
School of Physics & Astronomy
University of Birmingham
Birmingham B15 2TT, UK
E-mail: s.zhang@bham.ac.uk

X. Zhang, X. Su, Prof. C. Ouyang, Prof. J. Han, Prof. W. Zhang
Center for Terahertz Waves and College of Precision Instrument and Optoelectronics Engineering
Tianjin University
Tianjin 300072, China
E-mail: jiaghan@tju.edu.cn

N. Xu, Prof. W. Zhang
School of Electrical and Computer Engineering
Oklahoma State University
Stillwater, Oklahoma 74078, USA
E-mail: weili.zhang@okstate.edu

L. Liu, Prof. Y. Shi
Institute of Solid State Physics
Shanxi Datong University
Datong 037009, China

[+]These authors contributed equally to this work

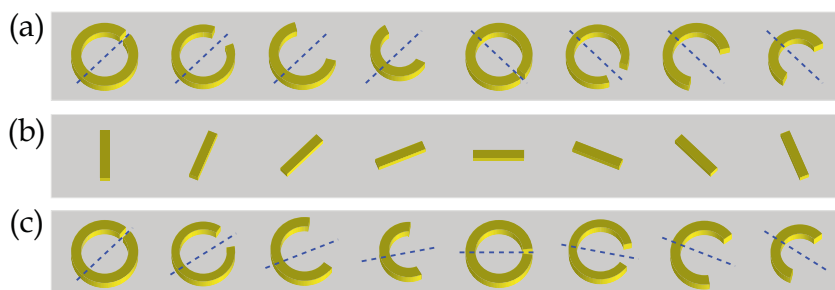© 2014 WILEY-VCH Verlag GmbH & Co. KGaA, Weinheim

Figure 1. Design of metasurfaces with simultaneous phase and amplitude control. (a) C-shaped antennas array with different geometrical parameters for phase control of linear polarization conversion. (b) Rod antennas array with different orientations for amplitude control of linear polarization conversion. Due to the duality between phase and amplitude, this type of metasurface also functions as a phase metasurface for a circular polarization incident beam. (c) C-shaped antennas array with same geometrical parameters corresponding to those in (a) but with different orientations as those in b for both phase and amplitude control of linear polarization conversion.

Sample Design: To implement this approach for controlling both phase and amplitude, we design a metasurface consisting of C-shaped antennas, as shown in **Figure 2**a. When a linearly polarized plane wave is incident onto a C-shaped antenna the symmetric $\tilde{E}_s$ and anti-symmetric $\tilde{E}_{as}$ modes are excited simultaneously (Figure 2a). The scattered fields from both the symmetric and anti-symmetric modes contribute to an orthogonally polarized output wave, whose phase and amplitude can be engineered by adjusting the shape parameters of the antenna.[14,35] When x-polarized wave $\tilde{E}_x^i$ is incident onto a C-shaped antenna with symmetry axis oriented along an arbitrary direction forming
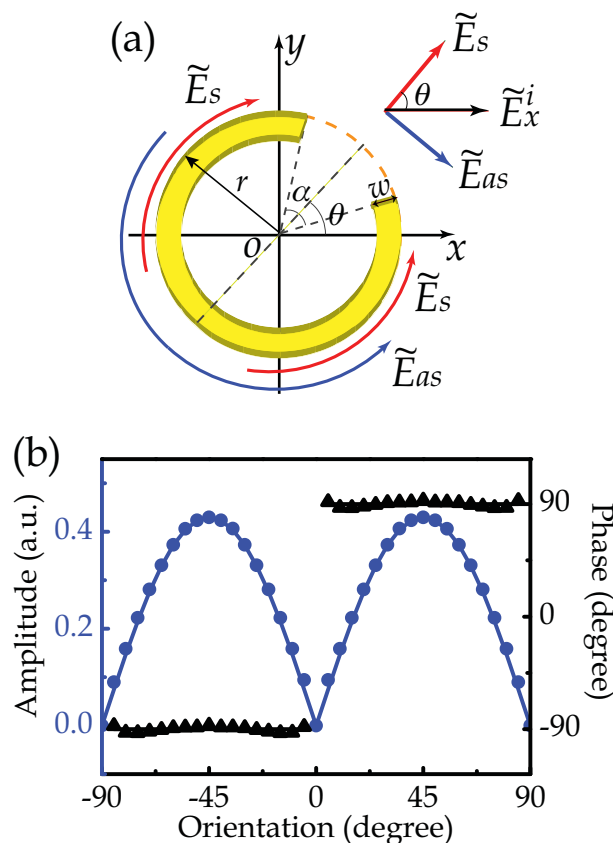
by the geometrical configuration of each antenna, and a metasurface for amplitude control realized by angular orientation manipulation. The metasurface of the first type consists of an array of C-shaped antennas, each one with carefully designed geometries. The metasurface operates in a linear cross-polarization scheme, i.e. the phase can be robustly controlled for a transmitted beam with a polarization orthogonal to that of the incident beam by their geometry – the arm length and the open angle (**Figure 1**a). These antennas operate in a similar manner to that of the widely adopted V-shaped antennas,[14,15] but can be designed to be more subwavelength. The symmetry line of each antenna is along +45° or −45° angle to maximise the conversion between the two linear polarizations in the horizontal and vertical directions.

The metasurface of the second type consists of an array of antennas with the same geometry but various orientations. Interestingly, there exists a duality between the phase and amplitude control in this type of metasurface – namely, the same metasurface works as a phase plate for a circularly polarized wave, or an amplitude plate for linear polarizations. For a linearly polarized incident beam, the scattering amplitude of the cross-polarization is continuously controlled by the orientation of each antenna.[14] This type of metasurface can also be employed for controlling the phase of the scattered wave in the cross circular polarization configuration (Figure 1b).[16] Combining the design concepts of these two types of metasurfaces leads to a metasurface consisting of an array of C-shaped antennas, whose phase and amplitude are separately controlled by their geometry and orientation (Figure 1c). Therefore, nearly arbitrary complex transmission/reflection coefficient distribution at the interface can be realized by simply arranging, in different orientation angles, the previously well studied V or C shape antennas, without having to specially design a new antenna for each combination of amplitude and phase. Thus, this approach represents a facile and robust way to obtain a metasurface with simultaneous phase control and continuously tunable amplitude profile, which greatly facilitates the complete control of light propagation.

Figure 2. Angular dependence of phase and amplitude of the antenna. (a) Schematic of C-shaped antenna with opening angle α, radius r, width w and orientation angle θ towards x-axis, where the red and blue arrows represent the symmetric mode $\tilde{E}_s$ $\tilde{E}_s$ and anti-symmetric mode $\tilde{E}_{as}$ $\tilde{E}_{as}$ of the antenna, respectively. Inset shows the geometric relationship used to calculate the scattered y-polarized wave under a normally incident x-polarized wave. (b) Simulated transmission amplitude (blue circle) and phase (black triangle) of an array of C-shaped antenna with $(r, \alpha) = (34\ \mu m, 11°)$ and θ varying from −90° to +90° at 0.63 THz. The amplitude profile follows a $|\sin(2\theta)|$ dependence (blue solid line), whereas the phase profile remains constant except for a π phase jump at $\theta = 0$. The period of the array is 80 μm in both x- and y-direction.

an angle θ with x axis (inset of Figure 2a), the generated γ-polarized scattered field $\tilde{E}_\gamma^s$ can be written as,[35]

$$\tilde{E}_\gamma^s = \frac{1}{2}\tilde{E}_x^i \sin(2\theta)\left(A_s e^{i\phi_s} + A_{as}e^{i\phi_{as}}\right) = \tilde{E}_x^i A e^{i\phi} \qquad (1)$$

where A_s, A_{as} and φ_s, φ_{as} denote the scattered amplitude and phase from the symmetric and anti-symmetric modes when the symmetry axis of the structure is along $\theta = 45°$, A and φ denote the overall scattered amplitude and phase, respectively. According to Equation (1), for a fixed antenna design, the amplitude of $\tilde{E}_\gamma^s$ is solely determined by the orientation angle θ. When the symmetry axis of the structure is along $\theta = 45°$, the amplitude of $\tilde{E}_\gamma^s$ reaches the maximum. On the other hand, varying the orientation angle θ of the symmetry axis of an antenna between 0° and 90° does not affect the phase of its scattered wave at all, whereas when θ is between 0° and –90°, only an additional π phase shift is incurred. Figure 2b shows the simulated amplitude and phase variations of a C-shaped antenna at different orientation angles from –90° to +90° at 0.63 THz, where the amplitude varies as $|\sin(2\theta)|$ while the phase remains constant in two separated ranges of –90° to 0° and 0° to +90°, with an abrupt change of π at $\theta = 0°$. Thus, the orientation angle θ serves as one important parameter to control the amplitude of a scattered wave without resorting to new antenna geometry.

This approach for realising metasurfaces with simultaneous control of phase and amplitude is applied to the design of terahertz metasurface gratings which can arbitrarily control the diffraction orders for a linearly polarized incident beam. To generate a grating with desired diffraction order amplitudes A_m, the transmission through the grating should be in general expressed as,

$$t(x) = A(x)\exp[i\phi(x)] = \sum_m A_m \exp(-i2m\pi x / d) \qquad (2)$$

where d is the grating periodicity and m is an integer denoting the diffraction order. For achieving a single diffraction order, the transmission function is simply a linear phase profile along x direction and a uniform amplitude. This is also referred to as anomalous refraction, which has been realized using a metasurface phase plate.[14,15] However, the amplitude of the transmission in general varies with x for generating multiple diffraction orders, which means that both the phase and amplitude need to be carefully controlled.

Three metasurface designs for generating different numbers of diffraction orders are given in **Figure 3**. All the metasurfaces contain four different antenna geometries,[35] whose phase evenly span the range from 0 to π at a step of $\pi/4$, and with a flip along the horizontal axis of each antenna to introduce an additional phase shift of π. As shown in Figure 3a, the supercell of the metasurface for generating a single diffraction order (–1st order) consists of eight antennas, whose symmetry axes are along either +45° or –45° to realize a linear phase profile between 0 and 2π and a constant amplitude profile. The supercells of the metasurfaces for generating two (–1st and –3rd) and three (–1st, –2nd and –3rd) diffraction orders consist of sixteen antennas, with the orientation of the symmetry axis of each
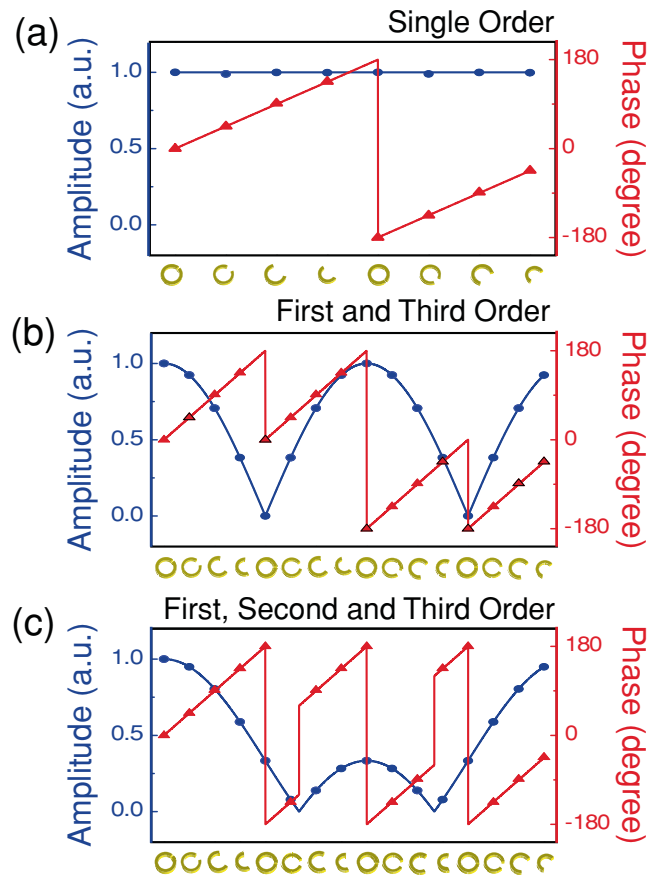
Figure 3. Amplitude and phase profiles of the diffractional metasurfaces. For each metasurface, four different C-shaped antennas are designed with the same $w = 5$ μm but different $(r, \alpha) = (34$ μm, $11°)$, $(32.3$ μm, $47°)$, $(34.4$ μm, $117°)$ and $(29.8$ μm, $140°)$. Simulated amplitude (normalized) and phase profiles along x-axis for samples of (a) a single diffraction order, (b) two diffraction orders, (c) three diffraction orders at 0.63 THz for transmitted γ-polarized wave under x-polarized normal incidence, where the symbols represent the simulated results and the solid lines represent the designed profiles based on Equation (2). In (a), the orientations of each individual antennas are either +45° or –45°, whereas in (b) and (c), the orientations vary between +45° or –45°. The antenna spacing (pixel size) is 80 μm in the simulation.

antenna continuously varying between –45° and +45° to achieve the desired phase and amplitude profiles (Figure 3b, c). In all the plots, the phase and amplitude profiles calculated from the simulation on the antennas agree very well with the designed profiles.

Experimental Results: To experimentally demonstrate our analysis, samples A-D are fabricated by conventional photolithography. Sample A, with an antenna spacing of 80 μm (supercell size = 640 μm × 80 μm), is designed to show a single diffraction order. Sample B and C are both designed for achieving two diffraction orders but with slightly different antenna spacings (100 μm for sample B and 80 μm for sample C). Sample D is designed for achieving three diffraction orders, which has an antenna spacing of 100 μm (supercell size = 1600 μm × 100 μm). The C-shaped antennas made of 200 nm thick aluminum are patterned on a silicon substrate. The optical images of the sample C and D are shown in **Figure 4**a,b, respectively.

**ADVANCED
MATERIALS**

www.advmat.de

**Materials
Views**

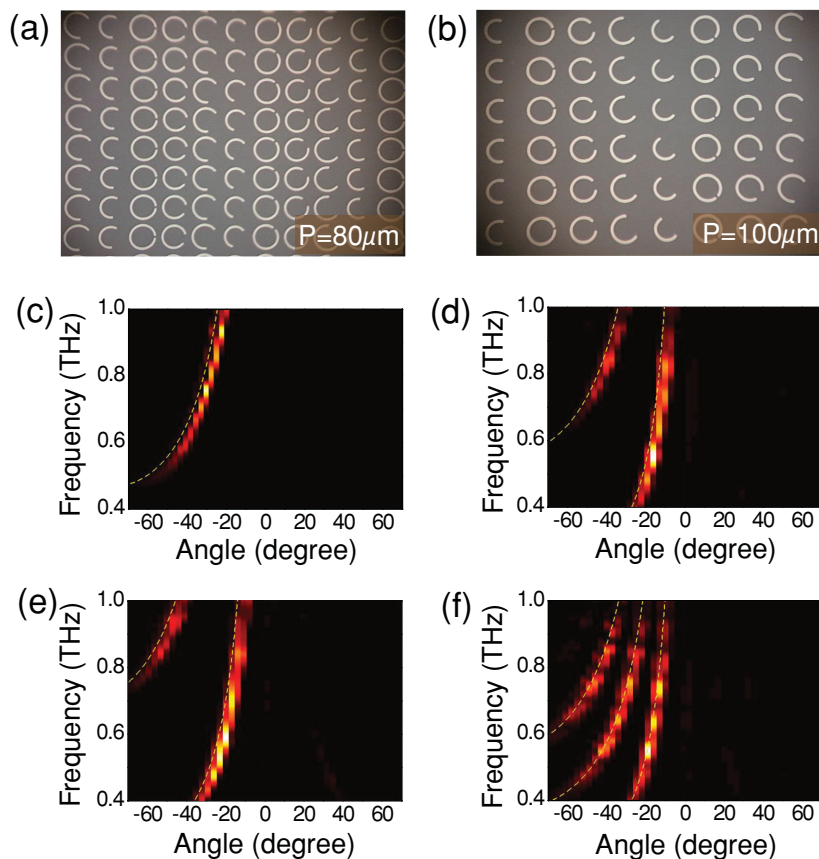www.MaterialsViews.com

COMMUNICATION

Figure 4. Experimental characterization of the metasurfaces at normal incidence. (a,b) Top view of the sample C and D, where *P* is the pixel size, i.e. the spacing between adjacent antennas. (c) Measured diffraction of sample A with amplitude and phase profile illustrated in Figure 3a and *P* = 80 μm. (d) Measured diffraction of sample B with amplitude and phase profile illustrated in Figure 3b and *P* = 100 μm, (e) Measured diffraction of sample C with amplitude and phase profile illustrated in Figure 3b and *P* = 80 μm. (f) Measured diffraction of sample D with amplitude and phase profile illustrated in Figure 3c and *P* = 100 μm. The yellow dashed lines represent the calculated diffraction angles.

The diffraction spectra of the sample D are dominated by three diffraction orders, which again agree very well with the design. For all the samples, the measured diffraction angles match very well with the theoretically calculated diffraction angles over the whole frequency range of 0.4 to 1.0 THz. The observed multiple diffraction orders in samples B, C and D directly confirm that the metasurfaces exhibit well controlled phase and amplitude profiles. It is noted that for those samples with multiple diffraction orders, the intensity of the lowest diffraction order is always stronger than that of the higher order ones, despite the metasurfaces being designed to have equal electric field between the multiple orders. This can be explained by the difference in the projection area of the metasurface along the propagation direction of the different diffraction orders: at larger diffraction angles, the projection area is smaller and consequently the overall energy carried by that diffraction order is smaller.

Numerical Simulation: 3D finite-difference-time-domain (FDTD) simulations are performed for the four samples by using commercially available software *CST Microwave Studio*. In the simulation, a terahertz beam is incident from the substrate side onto the metasurfaces. The simulated cross-polarized electric field distributions for terahertz transmitting through the metasurfaces at 0.8 THz, where all the designated diffraction orders can be seen, are shown by **Figure 5**.

Figure 5a shows the simulation results for sample A, where a uniform anomalous transmitted wave is observed, agreeing well with our design of a metasurface with a single diffraction order. Figure 5b, e, f show the simulation results for metasurfaces with two (sample B and C) and three (Sample D) diffraction orders, respectively. In these plots, the electric field distributions are no longer uniform due to the interference among multiple diffraction orders. In order to retrieve the information of the diffraction orders, Fourier Transformation is applied to the extracted field distributions along *x*-axis at a distance of 900 μm away from the metasurfaces. The results are shown in Figure 5c,d,g,h, where a single dominant diffraction order at $m = -1$ (Figure 5c), two dominant diffraction orders at $m = -1$ and -3 with different diffraction angles (Figure 5d,g), and three dominant diffraction orders at $m = -1$, -2 and -3 (Figure 5h) are observed for the three metasurfaces, respectively. The simulation results show very good agreement with the measurements.

To summarise, a design scheme for realizing metasurfaces capable of controlling both the phase and amplitude profile has been proposed. The design of the metasurface is simple, robust and broadband, and benefits from the freedom in engineering simultaneously the geometry and orientation angle of the
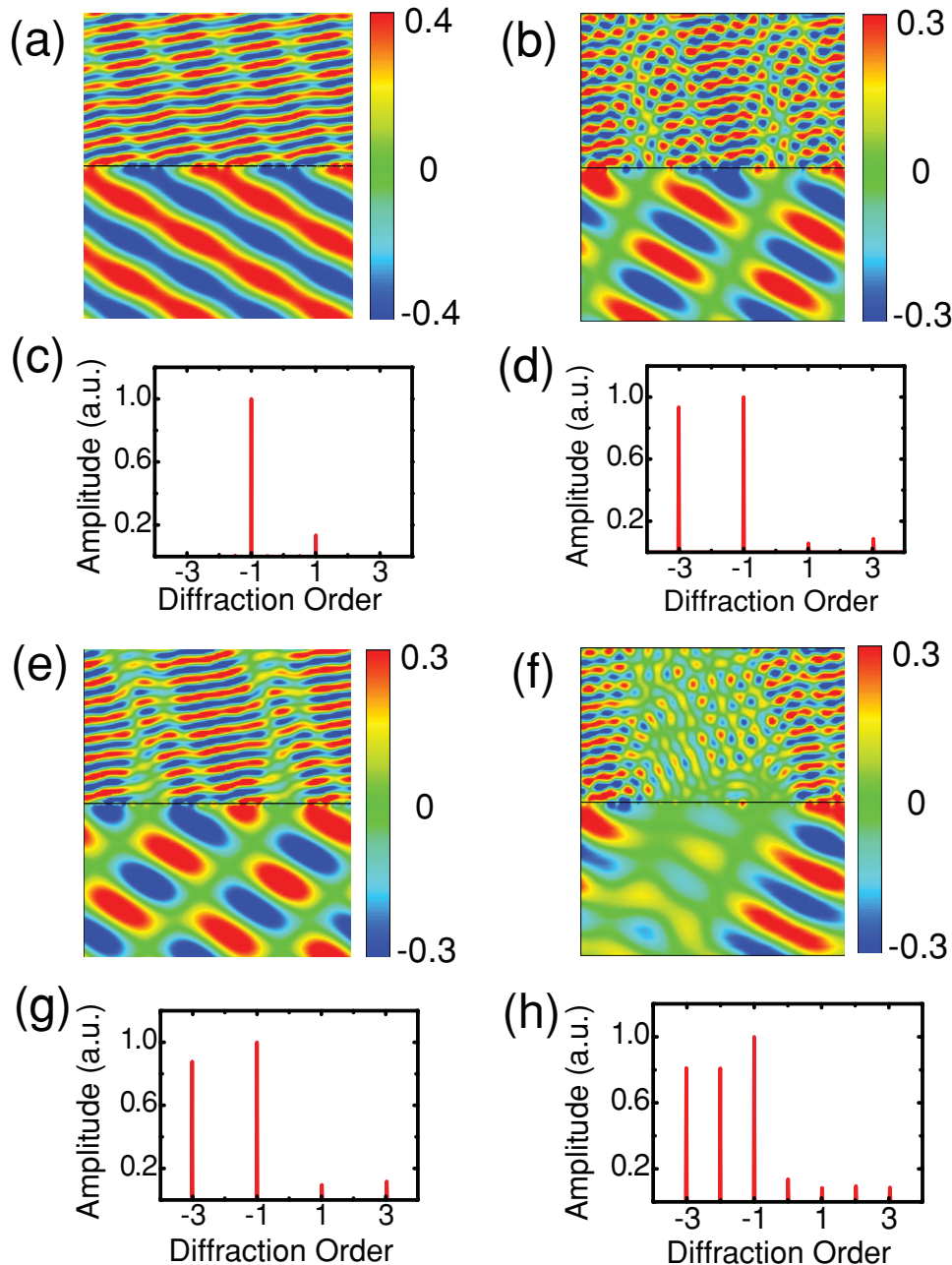
A fiber-based angular resolved terahertz time-domain spectroscopy (THz-TDS) is employed to characterise the diffraction orders of the samples in the range between 0.4 and 1.0 THz in a THz-TDS measurement at normal incidence (see Experimental Section).

The experimental results are shown in Figure 4c–f, where the diffraction spectra over the frequency range of 0.4 to 1.0 THz are shown in a broad angular range from –70° to +70°. Sample A clearly shows a single diffraction order, which is consistent with our previous work using the same metasurface design.[35] Although the metasurfaces are designed at 0.63 THz, it can be seen that a single diffraction order persists over a quite broad frequency range between 0.5 to 1.0 THz. The efficiency of anomalous refraction is estimated to be less than 20%. However it has been shown that by adding two layers of metallic gratings perpendicular to each other, one above and one below the metasurface, the efficiency can be dramatically enhanced.[23] As predicted by the design, sample B and C both exhibit two diffraction orders, but at different diffraction angles due to the slightly different pixel sizes (100 and 80 μm).

Figure 5. Simulated electric field distributions and the numerically retrieved diffraction orders. (a,b,e,f) Simulated *y*-polarized electric field distributions of for (a) sample A, (b) sample B, (e) sample C, and (f) sample D at 0.8 THz. The terahertz beam is incident from the side of the silicon substrate at normal incidence. (c,d,g,h) The corresponding diffraction order distribution calculated by Fourier transformation of the extracted *y*-polarized electric field distribution along *x*-axis at a distance of 900 μm from the metasurfaces in the air part. The antenna spacing is 80 μm in (a), (e) and 100 μm in (b), (f), to be consistent with the measurement.

antennas in the metasurface. As a proof of concept demonstration, we show that the design can be applied to realize a metasurface grating capable of arbitrarily controlling the intensity of each diffraction order. Our approach can be utilised to engineer complex holograms with simultaneous phase and amplitude control, which paves the way towards high quality computer generated holography, and the generation of arbitrarily complex optical patterns.

Experimental Section

The anomalous diffractions were measured by use of an angular resolved THz-TDS. The terahertz pulses transmitter and receiver were a pair of commercial fiber-based terahertz photoconductive switches (Menlon System). The terahertz wave emitted from the transmitter was first collected by a dielectric lens, then it was refocused to the receiver by a same lens after passing through the samples. Samples were placed in the center of a big rotation stage with the phase gradient along the horizontal direction, while the receiver was placed on a metal rail, which

is fixed on the rotation stage. It enables the receiver to detect any signal from the sample. Meanwhile, two polarizers were employed, one in front and one behind the sample, to improve the desired wave polarization; with horizontal polarization incidence and vertical polarization detection. The diffraction wave was detected every 3° by rotating the rotation stage from −90° to +90°.

Acknowledgements

[1] J. B. Pendry, *Phys. Rev. Let.* **2000**, *85*, 3966.

[2] R. A. Shelby, D. R. Smith, S. Schultz, *Science* **2001**, *292*, 77.

[3] S. Zhang, W. Fan, N. C. Panoiu, K. J. Malloy, R. M. Osgood, R. J. Brueck, *Phys. Rev. Lett.* **2005**, *95*, 137404.

[4] V. M. Shalaev, W. Cai, U. K. Chettiar, H. K. Yuan, A. K. Sarychev, V. P. Drachev, A. V. Kildishev, *Opt. Lett.* **2005**, *30*, 3356.

[5] M. Silveirinha, N. Engheta, *Phys. Rev. Lett.* **2006**, *97*, 157403.

[6] A. Alù, M. G. Silveirinha, A. Salandrino, N. Engheta, *Phys. Rev. B* **2007**, *75*, 155410.

[7] X. Huang, Y. Lai, Z. H. Hang, H. Zheng, C. T. Chan, *Nat. Mater.* **2011**, *10*, 582.

[8] N. Fang, H. Lee, C. Sun, X. Zhang, *Science* **2005**, *308*, 534.

[9] T. Taubner, D. Korobkin, Y. Urzhumov, G. Shvets, R. Hillenbrand, *Science* **2006**, *313*, 1595.

[10] Z. Liu, H. Lee, Y. Xiong, C. Sun, X. Zhang, *Science* **2007**, *315*, 1686.

[11] D. Schuig, J. J. Mock, B. J. Justice, S. A. Cummer, J. B. Pendry, A. F. Starr, D. R. Smith, *Science* **2006**, *314*, 977.

[12] J. Valentine, J. Li, T. Zentgraf, G. Bartal, X. Zhang, *Nat. Mater.* **2009**, *8*, 568.

[13] T Ergin, N. Stenger, P. Brenner, J. B. Pendry, M. Wegener, *Science* **2010**, *328*, 337.

[14] N. Yu, P. Genevet, M. A. Kats, F. Aieta, J. P. Tetienne, F. Capasso, Z. Gaburro, *Science* **2011**, *334*, 333.

[15] X. Ni, N. K. Emani, A. V. Kildishev, A. Boltasseva, V. M. Shalaev, *Science* **2012**, *335*, 427.

[16] L. Huang, X. Chen, H. Mühlenbernd, G. Li, B. Bai, Q. Tan, G. Jin, T. Zentgraf, S. Zhang, *Nano Lett.* **2012**, *12*, 5750.

[17] M. Kang, T. Feng, H. T. Wang, J. Li, *Opt. Exp.* **2012**, *20*, 15882.

[18] X. Yin, Z. Ye, J. Rho, Y. Wang, X. Zhang, *Science* **2013**, *339*, 1405.

[19] N. Shitrit, I. Yulevich, E. Maguid, D. Ozeri, D. Vesksler, V. Kleiner, E. Hasman, *Science* **2013**, *340*, 724.

[20] F. Aieta, *Nano Lett.* **2012**, *12*, 4932.

[21] X. Chen, L. Huang, H. Mühlenbernd, G. Li, B. Bai, Q. Tan, G. Jin, C. Qiu, S. Zhang, T. Zentgraf, *Nat. Commun.* **2012**, *3*, 1198.

[22] X. Ni, S. Ishii, A. V. Kildishev, V. M. Shalaev, *Lights: Science & Applications* **2013**, *2*, e72.

[23] N. K. Grady, J. E. Heyes, D. R. Chowdhury, Y. Zeng, M. T. Reiten, A. K. Azad, A. J. Taylor, D. A. R. Dalvit, H. T. Chen, *Science* **2013**, *340*, 1304.

[24] S. Sun, *Nat. Mater.* **2012**, *11*, 426.

[25] S. Sun, K. K. Yang, C. M. Wang, T. K. Juan, W. T. Chen, C. Y. Liao, Q. He, S. Xiao, W. T. Kung, G. Y. Guo, L. Zhou, D. P. Tsai, *Nano. Lett.* **2012**, *12*, 6223.

[26] J. Lin, J. P. B. Mueller, Q. Wang, G. Yuan, N. Antonious, X. C. Yuan, F. Capasso, *Science* **2013**, *340*, 331.

[27] L. Huang, X. Chen, B. Bai, Q. Tan, G. Jin, T. Zentgraf, S. Zhang, *Lights: Science & Applications* **2013**, *2*, e70.

[28] L. Huang, X. Chen, H. Mühlenbernd, H. Zhang, S. Chen, B. Bai, Q. Tan, G. Jin, K. W. Cheah, C. W Qiu, J. Li, T. Zentgraf, S. Zhang, *Nat. Commun.* **2013**, *4*, 2808.

[29] F. Zhou, Y. Liu, W. Cai, *Opt. Exp.* **2013**, *21*, 4348.

[30] W. T. Chen, K. Y. Yang, C. M. Wang, Y. W. Huang, G. Sun, I. D. Chiang, C. Y. Liao, W. L. Hsu, H. T. Lin, S. Sun, L. Zhou, A. Q. Liu, D. P. Tsai, *Nano Lett.* **2014**, *14*, 225.

[31] X. Ni, A. V. Kildishev, V. M. Shalaev, *Nat. Commun.* **2013**, *4*, 2807.

[32] J. Lin, P. Genevent, M. A. Kats, N. Antoniou, F. Capasso, *Nano Lett.* **2013**, *13*, 4269.

[33] M. Farmahini-Farahani, J. Cheng, H. Mosallaei, *J. Opt. Soc. Am. B* **2013**, *30*, 2365.

[34] N. Yu, F. Aieta, P. Genevet, M. A. Kats, Z. Gaburro, F. Capasso, *Nano Lett.* **2012**, *12*, 6328.

[35] X. Zhang, Z. Tian, W. Yue, J. Gu, S. Zhang, J. Han, W. Zhang, *Adv. Mater.* **2013**, *25*, 4567.

[36] P. Genvent, N. Yu, F. Aieta, J. Lin, M. A. Kats, R. Blanchard, M. O. Scully, Z. Gaburro, F. Capasso, *Appl. Phy. Lett.* **2012**, *100*, 013101.

[37] M. A. Kats, P. Genevet, G. Aoust, N. Yu, R. Blanchard, F. Aieta, Z. Gaburro, F. Capasso, *Proc. Natl. Acad. Sci. USA* **2012**, *109*, 12364.

[38] F. Monticone, N. M. Estakhri, A. Alù, *Phys. Rev. Lett.* **2013**, *110*, 203903.

[39] C. Pfeiffer, A. Grbic, *Phys. Rev. Lett.* **2013**, *110*, 197401.

[40] N. Yu, F. Capasso, *Nat. Mater.* **2014**, *13*, 139.

[41] Y. Yang, W. Wang, P. Moitra, I. I. Kravchenko, D. P. Briggs, J. Valentine, *Nano Lett.* **2014**, *12*, 1394.